Testing mean-field models near the $N=Z$ line: γ-ray spectroscopy of the $T_z=\frac{1}{2}$ nucleus ^{73}Kr

N. S. Kelsall,[1] S. M. Fischer,[2] D. P. Balamuth,[3] G. C. Ball,[4] M. P. Carpenter,[5] R. M. Clark,[6] J. Durell,[7] P. Fallon,[6] S. J. Freeman,[7] P. A. Hausladen,[3] R. V. F. Janssens,[5] D. G. Jenkins,[3,5,*] M. J. Leddy,[7] C. J. Lister,[5] A. O. Macchiavelli,[6] D. G. Sarantites,[8] D. C. Schmidt,[2] D. Seweryniak,[5] C. E. Svensson,[6,†] B. J. Varley,[7] S. Vincent,[9,‡] R. Wadsworth,[1] A. N. Wilson,[1,§] A. V. Afanasjev,[5,9,‖] S. Frauendorf,[9] I. Ragnarsson,[10] and R. Wyss,[11]

[1]*Department of Physics, University of York, Heslington, York Y010 5DD, United Kingdom*

[2]*Department of Physics, DePaul University, Chicago, Illinois 60614*

[3]*Department of Physics and Astronomy, University of Pennsylvania, Philadelphia, Pennsylvania 19104*

[4]*TRIUMF Laboratory, 4004 Westbrook Mall, Vancouver, British Columbia, Canada V6T 2A3*

[5]*Physics Division, Argonne National Laboratory, Argonne, Illinois 60439*

[6]*Nuclear Science Division, Lawrence Berkeley National Laboratory, Berkeley, California 94720*

[7]*Department of Physics, University of Manchester, Manchester M13 9PL, United Kingdom*

[8]*Department of Chemistry, Washington University, St. Louis, Missouri 63130*

[9]*Department of Physics, University of Notre Dame, Notre Dame, Indiana 46556*

[10]*Department of Mathematical Physics, Lund Institute of Technology, P.O. Box 118, S-22100 Lund, Sweden*

[11] *The Royal Institute of Technology, Physics Department Frescati, S-104 05 Stockholm, Sweden*

(Received 6 December 2001; published 5 April 2002)

Excited states in the $N=Z+1$ nucleus ^{73}Kr have been investigated using the ^{40}Ca(^{36}Ar,$2pn$) and ^{40}Ca(^{40}Ca,$\alpha 2pn$) reactions at 145 and 160 MeV, respectively. γ rays were detected using the Gammasphere array and events were recorded in coincidence with charged-particle and neutron detectors. The three previously observed bands were extended to high spin, and a new unfavored positive-parity band has been observed. The alignment characteristics and decay properties of the bands are all consistent with large-deformation prolate rotation, with no clear evidence for oblate bands or shape coexistence. This is quite different from neighboring ^{72,74}Kr, indicating a strong shape-stabilizing role for the valence neutron. The experimental results are compared to extended total Routhian surface, cranked Nilsson Strutinsky, and cranked relativistic mean-field calculations. The results suggest that the paired calculations lack some important physics. Neutron-proton correlations may be the missing ingredient. There is also evidence for an unusual band crossing in the negative-parity bands, which may indicate the presence of $T=0$ pairing correlations. At high spin all the models can reproduce the experimental data.

DOI: 10.1103/PhysRevC.65.044331 PACS number(s): 21.10.Re, 21.60.−n, 23.20.Lv, 27.50.+e

I. INTRODUCTION

Even-even nuclei with $A\sim 70$ lying at or close to the $N=Z$ line have been found to exhibit shape coexistence between highly deformed, near-degenerate oblate and prolate shapes. They are also interesting in the context of possible neutron-proton pairing correlations, which have been suggested to modify their properties. It is known from Nilsson calculations that large prolate and oblate shell gaps, ~ 2 MeV, exist for both neutrons and protons at $\beta_2 \sim +0.4$ (at particle numbers 38, 40) and at $\beta_2 \sim -0.3$ (at particle numbers 34, 36), respectively. This leads to large shape changes among nuclei in this region with the removal or addition of only one or two nucleons. For example, ^{72}Kr is believed to have an oblate ground state [1,2] with a low-lying prolate isomer [3], while in ^{74}Kr the situation is thought to be reversed, with a prolate ground state [4] and a low-lying oblate isomer [5,6]. Both oblate and prolate bands are seen to compete for yrast status in ^{68}Se [7]. Furthermore, in ^{74}Kr there is also evidence for a substantial reduction in deformation in the yrast band following the alignment of $g_{9/2}$ particles [8].

Investigating the odd-A nuclei in this region is important as it allows inference of the shapes of bands at low spin and permits the investigation of alignment blocking, and thus the destruction of pairing correlations, at higher spins. Detailed studies of ^{75}Kr by Skoda *et al.* [9,10] indicate that shape mixing plays an important role in these odd-A systems. In ^{73}Kr the minima in the potential energy surface have been predicted to be nearly degenerate, though with a substantial barrier between them, so shape mixing may be reduced. Determining whether oblate or prolate bands are yrast is one of the goals of this study.

Another question relates to the role of pairing in the structure of medium-heavy $N\sim Z$ nuclei. It has been widely suggested that near $N=Z$ neutron-proton, np, correlations may become important. Masses and excitation energies of iso-

*Present address: Department of Physics, University of Liverpool, Liverpool, L69 7ZE, UK.

†Present address: Department of Physics, University of Guelph, Guelph, Ontario, Canada N1G 2W1.

‡Present address: Physics Department, University of Surrey, Guildford, Surrey GU2 7XH, UK.

§Present address: Department of Nuclear Physics, Australian National University, Canberra ACT0200, Australia.

‖On leave of absence from Laboratory of Radiation Physics, Institute of Solid State Physics, University of Latvia, LV 2169 Salaspils, Miera str. 31, Latvia.

baric analog states have been interpreted in different ways. Macchiavelli *et al.* [11,12] argued that the data on binding energies and the energies of isobaric analog states can be understood as a consequence of isovector ($T=1$) pairing, containing the np part that is necessary to conserve isospin. In addition, Frauendorf and Sheikh [13] demonstrated that some aspects of rotational spectra in $N\sim Z$ nuclei can be interpreted in terms of a cranked shell model that is based on quasiparticles belonging to a pure isovector pair field. On the other hand, Satuła and Wyss [14,15] suggest that there is evidence for isoscalar ($T=0$) np pairing effects in the energies of low-lying states of $N=Z$ nuclei. In their mean-field calculations, the presence of an isoscalar pair field is able to account for the binding energies (Wigner term) and the excitation energies of the $T=1$ and $T=0$ states [15,16]. Moreover, recent work on ^{72}Kr, ^{76}Sr, ^{80}Zr, and ^{88}Ru [17–19] has observed large delays (compared to heavier even-even isotopes) in the crossing frequencies of the aligning $g_{9/2}$ protons and neutrons. In the early work of de Angelis *et al.* [2] on ^{72}Kr this was interpreted as evidence for strong $T=0$ pairing correlations in the ground state. It is unclear, however, as to whether $T=1$ or $T=0$, or a combination of both types of np pair correlations is responsible for the observed delay in these nuclei. Frauendorf and Sheikh [13] found that isovector ($T=1$) np correlations can shift the band crossings to higher frequencies. However, as a result of the limitations of their j-shell model it was not possible to judge if the effect is strong enough to explain the shift in real nuclei. More recent work suggests that the delay in crossing frequency cannot be understood if only $T=1$ pairing is included within current mean-field models (e.g., see [20]). In addition, it has been shown that a static $T=0$ pair field can result in an increase in the crossing frequency [21,22] (see also [18]).

Theoretically, np pairing effects are expected to diminish rapidly as one departs from the $N=Z$ nuclei. This has been used as an explanation of why total Routhian surface (TRS) model calculations, using standard $T=1$ like-nucleon pairing, can reproduce the experimental data for the $T_z=1$ nuclei ^{74}Kr, ^{78}Sr, and ^{82}Zr [4]. However, such an argument may be too superficial, because strong $T=1$ np pair correlations show up in a subtle way, as a result of the breaking of isospin symmetry by the isovector pair field. Reference [13] demonstrated that single-j-shell calculations, using only standard $T=1$ like-nucleon pairing, can reproduce the spectrum of the $N=Z$ nucleus ^{74}Rb if isospin conservation is taken into account (which accounts for the $T=1$ np pair correlations). Previous studies of the odd-proton nuclei ^{75}Rb [23] and ^{79}Y [24] have also indicated that TRS calculations can explain the observed data in these $T_z=\frac{1}{2}$ nuclei. In addition, in Ref. [24] it was also stated that if $T=0$ np pairing is present, then this does not appear to significantly affect simple observables such as the moments of inertia of the rotational bands at low spins. In ^{75}Rb some small differences were observed between experiment and theory in the band crossing region. The authors noted that this in itself was not explicit proof of np correlations, but suggested that if they were significant, they most likely arise from isoscalar residual np interactions. At present it is not at all clear what the true nature of the np pair correlations is in nuclei near the $N=Z$ line or how these are revealed in rotational spectra. Detailed low-spin and high-spin experimental data in medium-heavy $T_z=\pm\frac{1}{2}$ nuclei will be extremely important in helping to clarify this complex issue.

A further interesting aspect of this mass region has been the observation of bands which show characteristics that are generally associated with smoothly terminating bands [25]. In ^{81}Sr [25,26] the structures do not appear to become fully noncollective at the highest spins, but in ^{73}Br [27] one of the rotational bands is observed up to its terminating single-particle state at a spin of $\frac{63}{2}$.

The present work concerns the γ-ray spectroscopy of the $T_z=\frac{1}{2}$ nucleus ^{73}Kr. After some initial misidentification [28,29], the Cologne group [30] identified three excited bands associated with ^{73}Kr and inferred that the ground-state quantum numbers were $I^\pi=\frac{5}{2}^-$, based on β decay to known states in ^{73}Br. Recently, two studies have revised the ground-state and low-lying ^{73}Kr spin assignments. A detailed off-line decay study unambiguously fixed the ground-state spin and parity to be $I^\pi=\frac{3}{2}^-$ [31]. Further, an isomer was found [32] in a fragmentation reaction. Its decay populated the low-lying levels in ^{73}Kr and clarified the location and spins of the bandheads. However, the placement of the cascades of γ rays observed by Freund *et al.* [30] has been verified in the present work, as were most of the high-spin extensions suggested by Hausladen [33], although in both cases the spin sequences have been modified due to the ground-state reassignment. As we will discuss, the present spin arrangement is now consistent with the observed population of the high-spin bands.

II. EXPERIMENTAL DETAILS AND DATA REDUCTION

The data were obtained from two experiments performed using the ATLAS facility at Argonne National Laboratory. Excited states in the ^{73}Kr nucleus were populated in the ^{40}Ca(^{40}Ca,$\alpha 2pn$) and ^{40}Ca(^{36}Ar,$2pn$) reactions at beam energies of 160 MeV and 145 MeV, respectively. In each case, the target consisted of a $\sim$400-μg/cm^2-thick ^{40}Ca foil with 100 μg/cm^2 flashes of Au in front and behind to prevent oxidization of the Ca foil. Emitted γ rays were detected with the Gammasphere array [34]. As a result of the small cross section for the production of nuclei far from stability in this reaction, ancillary detectors were included in the experimental setup. These were the Microball CsI detector array [35] for the detection of protons and α particles, and an array of 30 liquid scintillation counters for the detection of neutrons. Data were collected using two trigger conditions: requiring at least two suppressed Ge detectors firing in coincidence with one or more events detected in the neutron shell or requiring more than four suppressed Ge detectors firing in prompt coincidence. The events in the neutron detectors were subsequently identified as neutrons (or γ rays) in software. The two reactions populated ^{73}Kr at different spins and excitation energies. The argon-induced reaction populated the nucleus at higher spin and allowed the bands to be extended furthest. The calcium-induced reaction populated lower spins, which was useful in ordering the γ rays in the

backbend region and also populated nonyrast states more favorably.

In the $A\sim70$ region the emission of light charged particles from the compound nucleus results in a substantial broadening of the recoil cone of the final reaction products. This has the effect of worsening the effective resolution of the γ-ray array. However, by using information from the Microball array, a full kinematic reconstruction can be performed [36] and much of the intrinsic resolution regained. Such an event-by-event Doppler reconstruction was employed in the analysis of data from both experiments.

Data from the $^{40}Ca+^{40}Ca$ experiment were sorted into a $\gamma\gamma$ coincidence matrix with the requirement that one α particle, two protons, and one neutron be detected in each event. Feedthrough from other reaction channels involving higher-multiplicity particle emission was subtracted in the analysis. Particle-gated angular distributions were also analyzed. Sums of single γ gates within the band(s) of interest were used in order to obtain cleaner spectra. This was essential particularly for analyzing the 200–300 keV crossover transitions in order to remove γ rays produced in reactions of ^{40}Ca on the ^{12}C target contaminant. The gates contained events from γ-ray detectors located at all available angles so as to minimize correlation effects. Angular distributions for the strongest in-band transitions were analyzed initially, with each displaying the characteristic quadrupole radiation pattern. The alignment parameter σ, representing a Gaussian distribution of magnetic substates, was allowed to vary in each case. A mean value for σ/I_i, where I_i is the spin of the initial state, was determined to be 0.42. This value was held fixed for the final analysis of all angular distribution measurements. Mixing ratios were extracted for several of the $\Delta I=1$ crossover transitions.

Data from the $^{36}Ar+^{40}Ca$ reaction were sorted off line into a E_γ-E_γ-E_γ cube with particle gates of one or two protons, zero alphas, and a single neutron in an attempt to enhance the ^{73}Kr channel relative to more strongly produced reaction products. These data were subsequently analyzed using the RADWARE suite of programs [37]. The data were also unpacked into triples events and directional correlation from oriented states (DCO) [38] E_γ-E_γ matrices were sorted. Three such matrices were created. Gates were set on individual γ rays from a list of transitions in ^{73}Kr (one list for each of bands 1–3). There was no restriction placed upon the angle of detection of the transitions in these lists so as not to bias the correlations. In addition, the same particle gates as discussed above were also utilized. The DCO matrices were constructed from the remaining two γ rays in the triples events using detectors from the 79°–101° rings on the x axes and all other detectors on the y axes. These data were used to extract the multipolarities of the transitions within and between the three observed bands. DCO ratios for known stretched quadrupole↔stretched quadrupole transitions were found to be ~1.1 on average, and those for stretched quadrupole↔stretched dipole transitions were found to be ~0.8. The ratios extracted for the in-band transitions in ^{73}Kr are consistent with those expected for quadrupole γ rays and with the measured angular distributions.

III. ANALYSIS

A. Decay schemes

The level scheme shown in Fig. 1 results from the analysis of the data obtained in the present work. Data from the $^{36}Ar+^{40}Ca$ reaction made it possible to significantly extend the previously known structures (bands 1, 2, and 3). The two negative-parity bands (labeled as bands 1 and 2 in Fig. 1) have been extended by ten and nine transitions up to tentative spins of $(\frac{63}{2}^-)$ and $(\frac{61}{2}^-)$, respectively. The previously observed positive-parity band (band 3) has also been extended by nine transitions up to a tentative spin of $(\frac{57}{2}^+)$. The spectra in Fig. 2 were obtained from setting different gating conditions within the particle-gated cube. Figures 2(a) and 2(b) show the spectra created from a sum of double gates in the RADWARE cube, details of which can be found in the figure caption. They illustrate the two signatures of the strongly coupled negative-parity sequence of transitions. Figure 2(c) gives a similar spectrum, created from a different sum of double gates within the RADWARE cube, for the positive-parity band 3 (see figure caption for details). In addition, a new band (band 4) which appears to be the signature partner to band 3, has been observed for the first time. The doublet nature of four of the transitions (714, 826, 1202, and 1207 keV) in this band makes the determination of the intensities rather difficult. However, placement of many of the transitions within the band is fixed by the observation of γ rays which link the new band to band 3. Figure 3 shows a particle-gated γ-ray spectrum from the Ca+Ca data that includes a sum of single gates on the 632, 1045, 1202, and 1354 keV transitions in band 4. The crossover transitions are identified as well as several transitions in the signature-partner band 3. The ordering of the last two observed transitions of 1354 and 1207 keV is uncertain. Finally, a short sequence of γ rays, comprised of the 1417 and 1498 keV transitions, which decay to the $\frac{23}{2}^-$ state in band 1, has also been observed.

The ordering of the transitions within the bands has been deduced mainly from γ-ray intensities measured in the coincidence data. ^{73}Kr was produced at substantially lower angular momentum in the $^{40}Ca+^{40}Ca$ reaction than in the $^{36}Ar+^{40}Ca$ reaction. This is fortuitous as data from the former reaction make it possible to order the transitions through the backbend region for bands 1, 2, and 3, while in the latter reaction the ordering is ambiguous. Table I contains information on the energies and intensities of the γ rays observed in the two experiments. In each case, the intensities are normalized relative to the intensity of the 144 keV transition. Evidence for the difference in population between the two reactions can be seen by comparing the intensities of the 827, 913, and 892 keV transitions in the two reactions. The intensities of the 827 keV and 913 keV transitions of the negative-parity bands 1 and 2 are very similar for the two reactions. In contrast, while the relative intensity of the 892 keV transition of the positive-parity band 3 is 95(4) in the $^{40}Ca+^{40}Ca$ reaction, it is only 54(7) in the $^{36}Ar+^{40}Ca$ reaction. Because of this difference in entry population, the unfavored positive-parity signature partner (band 4) was ob-

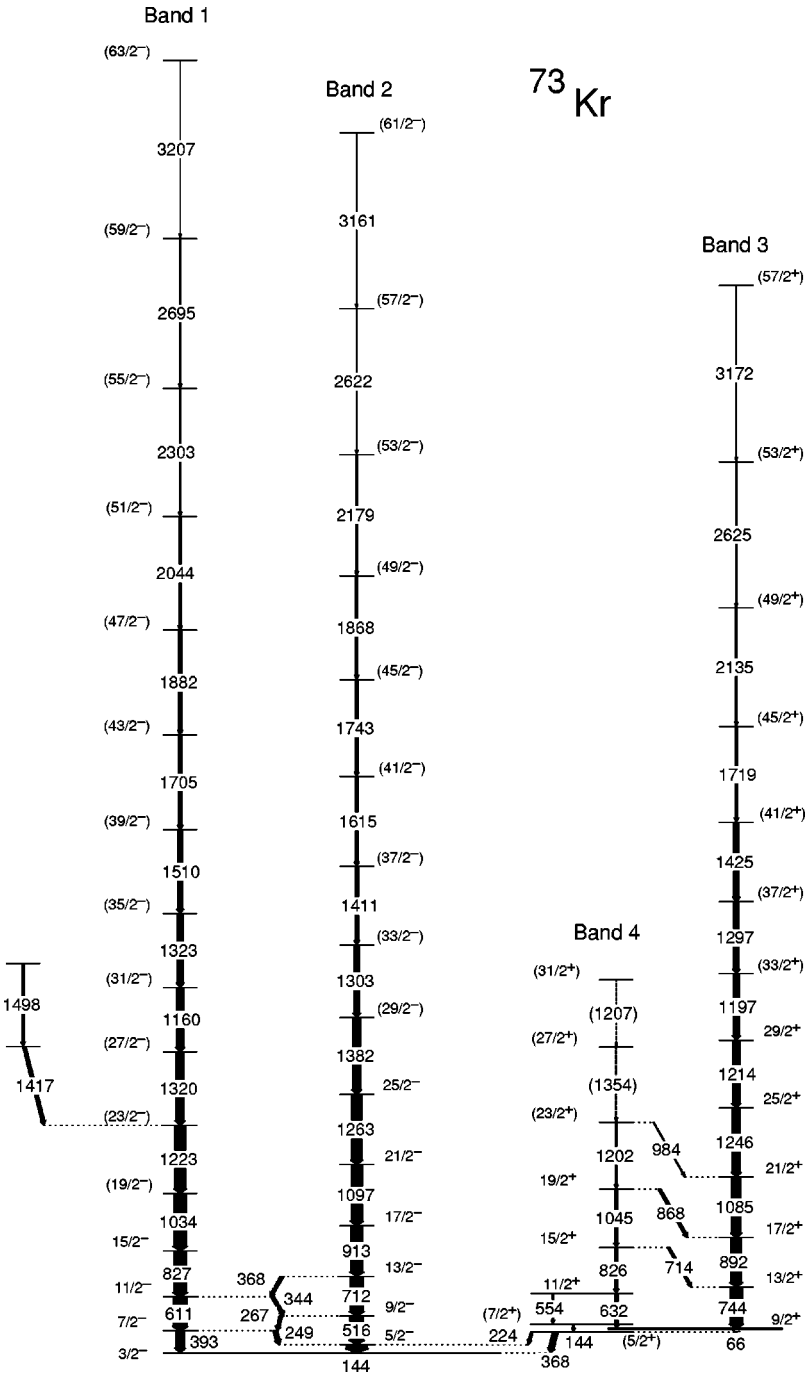

FIG. 1. Proposed level scheme for ^{73}Kr deduced from the present work.

served only in the ^{40}Ca + ^{40}Ca data.

The spin assignments adopted in this work are consistent with the the relative intensities of the positive- and negative-parity bands and how high in spin each can be traced. Figure 4(a) shows a plot of the level energy minus a rigid rotor reference energy as a function of spin for bands 1–3 using the spins assigned in the present work. Figure 4(b) shows the same plot with the spins of all the negative-parity states down to the 144 keV level reduced by $1\hbar$ (i.e., with the spins now the same as the assignments proposed in Ref. [30]). From these figures it is clear that the spins proposed in the present work are consistent with the observed feeding profile of the bands; i.e., the negative-parity states are yrast at high spin and should therefore be observed to higher spin than the positive-parity $\nu g_{9/2}$ structure.

B. Angular distributions

In the papers of Skoda *et al.* [9,10] on the shapes of bands in ^{75}Kr considerable attention was paid to measuring multipole mixing ratios $\delta(E2/M1)$ and branching ratios of the in-band decays in order to extract information on shape coexistence. The mixing ratios were independently extracted from the angular distributions and branching ratios. The analysis was inconsistent with the properties of strongly coupled bands having a constant quadrupole moment, as the mixing ratios extracted from angular distributions were dif-

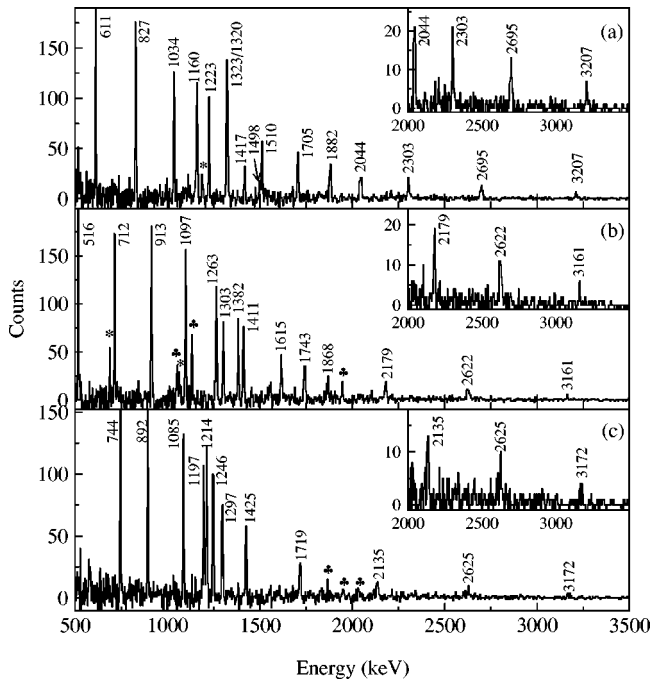

FIG. 2. Double-gated spectra created within an E_γ-E_γ-E_γ cube showing the three extended rotational bands in ^{73}Kr. (a) and (b) show the two negative-parity, signature-partner, bands 1 and 2, respectively. These were created from the particle-gated cube via a sum of gates contained within a list. A separate list was used for each band with γ rays from levels up to spins $\frac{55}{2}$ and $\frac{53}{2}$ being included for bands 1 and 2, respectively. (c) Shows the positive-parity band, band 3. Again this spectrum was created in the particle-gated cube from a sum of double gates included in a list which contained all γ rays within the band from levels up to spin $\frac{49}{2}$. Peaks marked with an * or ♣ denote contaminants from ^{71}Se and ^{72}Br, respectively.

ferent from those inferred from branching ratios. A rather complicated mixing of oblate and prolate shapes was suggested to explain this observation, with the $\Delta I=1$ and $\Delta I=2$ $E2$ matrix elements having different quadrupole strengths. We have studied the analogous ^{73}Kr interband

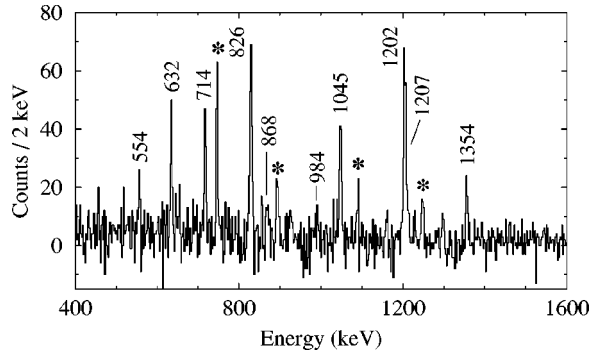

FIG. 3. Particle-gated γ-ray spectrum obtained from a sum of single gates on the 632, 1045, 1202, and 1354 keV transitions of band 4 in ^{73}Kr. The 714, 868, and 984 γ rays are crossover transitions to band 3. Peaks marked with an asterisk (*) are members of band 3.

transitions to see if the trends persist. We have measured the particle-gated angular distributions and branching ratios of the four $\Delta I=1$ decays in the negative-parity sequence and of two decays in the positive-parity sequence. Each analysis has some model dependence, concerning the alignment for angular distributions and concerning the strong coupling assumption for the branching ratio analysis. The results are summarized in Fig. 5 and Table II.

For the negative-parity sequence, based on the $I^\pi=\frac{3}{2}^-$ ground state, fits to the 249, 267, 344, and 368 keV angular distributions all have similar, positive, multipole mixing ratios (in the convention of Krane and Steffen [39]), indicating that the ratio of the band's magnetic moment to quadrupole moment, $(g_k-g_r)/Q$, should also be positive [40]. The magnetic factor can be calculated by recourse to the Nilsson model or any similar deformed shell model, so in principle both the sign and size of the deformation can be extracted and compared to TRS predictions. This has been shown to work well for the highly deformed rotors in this region [41]. For a prolate shape, the Nilsson orbit with $I^\pi=\frac{3}{2}^-$ near the $N=37$ Fermi surface is the $[312]\frac{3}{2}$ level, which has amplitudes dominated by the folded $(j=l-\frac{1}{2})$ $f_{5/2}$ shell model state. For prolate deformations with $\beta_2\sim+0.35$, a value of $g_k-g_r\sim+0.2\mu_n$ is obtained, resulting in an average quadrupole moment of $Q=+2.5(8)e$ b. The uncertainty in this mean quadrupole moment measurement arises from the uncertainty on the individual extracted mixing ratios (Table II), from the model-dependent estimate of the gyromagnetic moment, (g_k-g_r), and from the weighted average of the measurements from individual transitions. The low mixing ratio value for the 249 keV transition may arise from mismodeling the nuclear alignment; at the bottom of long cascades in thin target experiments using Gammasphere we have evidence of vacuum deorientation. The branching ratio analysis based on the strong-coupling limit with $K=\frac{3}{2}$ and a band with constant quadrupole moment indicates very similar mixing ratios, with the exception of the 249 keV transition, and again an average quadrupole moment of $|Q|=2.4(7)e$ b. These extracted quadrupole moments are slightly lower than that expected for a uniformly charged spheroid with $\beta_2\sim+0.35$, for which $Q=+2.6e$ b. However, in light of the large systematic uncertainties the agreement between methods of extracting δ is quite satisfactory, unlike the case of ^{75}Kr [10], and no shape-mixing arguments appear to be necessary. A similar analysis can be followed for oblate shapes with deformation $\beta_2\sim-0.3$. Here, there is a different $I^\pi=\frac{3}{2}^-$ level near the Fermi surface, and the calculated magnetic moment is large and negative, $g_k-g_r\sim-0.8\mu_n$ arising mainly from stretched $(j=l+\frac{1}{2})$ $f_{7/2}$ and $p_{3/2}$ components. Combining this magnetic moment with the measured mixing ratio leads to unphysically large quadrupole moments of $Q\sim-10e$ b, though with the self-consistent, negative sign. Consequently, oblate deformation for the negative-parity states is highly unlikely.

Assuming that band 4 is the signature partner to band 3, then the $g_{9/2}$ band has significant signature splitting, so the strong-coupling limit is open to question. However, the 714 and 868 keV $\Delta I=1$ decays have similar angular distribu-

TABLE I. Spectroscopic details for the γ-ray transitions in the four rotational bands observed in the present work. DCO ratios are given for those transitions for which statistics and contaminants allowed a ratio to be extracted. Firm spin assignments are based on measured DCO ratios and/or γ-ray angular distributions.

E_γ (keV)	I_{rel} (%) ^{40}Ca+^{40}Ca	I_{rel} (%) ^{36}Ar+^{40}Ca	DCO	$I_i^\pi(\hbar)$	$I_f^\pi(\hbar)$
144.0(1)	100(4)	100(5)	0.77±0.11	$\frac{5}{2}^-$	$\frac{3}{2}^-$
224(1)	7(2)			$\frac{5}{2}^+$	$\frac{5}{2}^-$
249.0(2)	24(6)	23(12)	0.76±0.06	$\frac{7}{2}^-$	$\frac{5}{2}^-$
267.1(3)	6(3)	17(5)	0.63±0.05	$\frac{9}{2}^-$	$\frac{7}{2}^-$
343.6(8)	5(2)			$\frac{11}{2}^-$	$\frac{9}{2}^-$
368.4(6)	4(2)			$\frac{13}{2}^-$	$\frac{11}{2}^-$
393(1)	59(2)	43(6)	0.97±0.10	$\frac{7}{2}^-$	$\frac{3}{2}^-$
516.1(1)	68(2)	68(12)	0.91±0.07	$\frac{9}{2}^-$	$\frac{5}{2}^-$
554.3(5)	7(4)			$\frac{11}{2}^+$	$(\frac{7}{2}^+)$
611.0(1)	58(6)	68(11)	1.26±0.18	$\frac{11}{2}^-$	$\frac{7}{2}^-$
632.3(4)	16(3)			$\frac{11}{2}^+$	$\frac{9}{2}^+$
712.1(1)	71(14)	67(10)	1.17±0.10	$\frac{13}{2}^-$	$\frac{9}{2}^-$
714.3(4)	12(5)			$\frac{15}{2}^+$	$\frac{13}{2}^+$
744.1(2)	99(4)	63(7)	1.00±0.2	$\frac{13}{2}^+$	$\frac{9}{2}^+$
826.2(5)	<20			$\frac{15}{2}^+$	$\frac{11}{2}^+$
826.7(2)	61(4)	66(8)	1.4±0.3	$\frac{15}{2}^-$	$\frac{11}{2}^-$
867.8(4)	14(5)			$\frac{19}{2}^+$	$\frac{17}{2}^+$
892.0(2)	95(4)	54(7)	0.94±0.05	$\frac{17}{2}^+$	$\frac{13}{2}^+$
913.0(1)	64(4)	63(10)	0.94±0.09	$\frac{17}{2}^-$	$\frac{13}{2}^-$
984(1)	<5			$(\frac{23}{2}^+)$	$\frac{21}{2}^+$
1034.0(2)	63(6)	63(9)	-	$(\frac{19}{2}^-)$	$\frac{15}{2}^-$
1045.3(6)	<20			$\frac{19}{2}^+$	$\frac{15}{2}^+$
1085.4(2)	75(4)	49(6)	1.7±0.2	$\frac{21}{2}^+$	$\frac{17}{2}^+$
1097.1(1)	61(2)	56(8)	0.90±0.13	$\frac{21}{2}^-$	$\frac{17}{2}^-$
1160.0(3)	14(2)	36(6)	-	$(\frac{31}{2}^-)$	$(\frac{27}{2}^-)$
1197.0(2)	33(4)	30(6)	-	$(\frac{33}{2}^+)$	$\frac{29}{2}^+$
1202(1)	<10			$(\frac{23}{2}^+)$	$\frac{19}{2}^+$
1207(3)	<5			$(\frac{31}{2}^+)$	$(\frac{27}{2}^+)$
1213.9(3)	37(4)	40(5)	1.55±0.4	$\frac{29}{2}^+$	$\frac{25}{2}^+$
1223.1(2)	42(4)	55(7)	1.7±0.3	$(\frac{23}{2}^-)$	$(\frac{19}{2}^-)$
1246.1(2)	48(4)	35(6)	0.90±0.2	$\frac{25}{2}^+$	$\frac{21}{2}^+$
1263.1(2)	34(4)	52(8)	1.22±0.15	$\frac{25}{2}^-$	$\frac{21}{2}^-$
1297.0(3)	19(4)	28(4)	2.09±0.5	$(\frac{37}{2}^+)$	$(\frac{33}{2}^+)$
1303.0(3)	9(2)	29(6)	1.44±0.3	$(\frac{33}{2}^-)$	$(\frac{29}{2}^-)$
1319.9(2)	18(6)	29(6)	-	$(\frac{27}{2}^+)$	$(\frac{23}{2}^-)$
1323.1(2)	11(6)	42(7)	1.04±0.13	$(\frac{35}{2}^-)$	$(\frac{31}{2}^-)$
1354(2)	<5			$(\frac{27}{2}^+)$	$(\frac{23}{2}^+)$
1382.0(4)	17(4)	40(8)	-	$(\frac{29}{2}^-)$	$\frac{25}{2}^-$
1411.0(6)	10(2)	18(5)	1.03±0.16	$(\frac{37}{2}^-)$	$(\frac{33}{2}^-)$
1416.9(4)	12(2)	17(4)	-	-	$(\frac{23}{2}^-)$
1425.0(5)	11(2)	27(4)	1.5±0.3	$(\frac{41}{2}^+)$	$(\frac{37}{2}^+)$
1497.5(7)		11(3)	-	-	-
1510.0(3)		24(5)	1.4±0.3	$(\frac{39}{2}^-)$	$(\frac{35}{2}^-)$

TABLE I. (*Continued.*)

E_γ (keV)	I_{rel} (%) ^{40}Ca+^{40}Ca	I_{rel} (%) ^{36}Ar+^{40}Ca	DCO	$I_i^\pi(\hbar)$	$I_f^\pi(\hbar)$
1615.1(4)		14(5)	-	$(\frac{41}{2}^-)$	$(\frac{37}{2}^-)$
1704.8(5)		18(3)	-	$(\frac{43}{2}^-)$	$(\frac{39}{2}^-)$
1719.0(6)		11(3)	-	$(\frac{45}{2}^+)$	$(\frac{41}{2}^+)$
1743.1(5)		11(2)	-	$(\frac{45}{2}^+)$	$(\frac{41}{2}^+)$
1868.1(7)		10(3)	-	$(\frac{49}{2}^-)$	$(\frac{45}{2}^-)$
1882.0(6)		14(3)	-	$(\frac{47}{2}^-)$	$(\frac{43}{2}^-)$
2043.9(6)		11(2)	-	$(\frac{51}{2}^-)$	$(\frac{47}{2}^-)$
2135(1)		6(2)	-	$(\frac{49}{2}^+)$	$(\frac{45}{2}^+)$
2179.0(7)		7(3)	-	$(\frac{53}{2}^-)$	$(\frac{49}{2}^-)$
2303(1)		5(2)	-	$(\frac{55}{2}^-)$	$(\frac{51}{2}^-)$
2622(2)		3(2)	-	$(\frac{57}{2}^-)$	$(\frac{53}{2}^-)$
2625(5)		4(1)	-	$(\frac{53}{2}^+)$	$(\frac{49}{2}^+)$
2695(1)		5(1)	-	$(\frac{59}{2}^-)$	$(\frac{55}{2}^-)$
3161(9)		1(1)	-	$(\frac{61}{2}^-)$	$(\frac{57}{2}^-)$
3172(8)		1(1)	-	$(\frac{57}{2}^+)$	$(\frac{53}{2}^+)$
3207(4)		1(1)	-	$(\frac{63}{2}^-)$	$(\frac{59}{2}^-)$

tions which are quite different from the decays in the negative-parity band (see Fig. 5). They can be fit only by negative multipole mixing ratios. For all shapes, this wave function is the stretched spherical $g_{9/2}$ state with $g_k - g_r \sim -0.8\mu_n$. Consistency with the sign of the mixing ratios can only be obtained for a prolate shape, with a calculated mean deformation of $Q = +3.0(10)e$ b. In the branching ratio analysis, the extracted value of δ is sensitive to the projection of angular momentum on the symmetry axis, K. Only for $K = \frac{5}{2}$ can agreement between the mixing ratio from angular distributions and that from branching ratios be

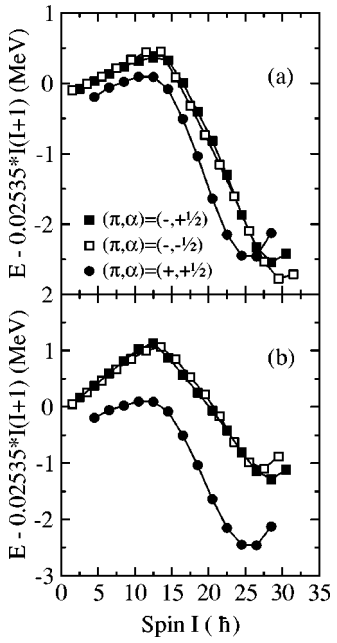

FIG. 4. (a) Plot of experimental level energies minus a rigid rotor reference as a function of spin for bands 1 to 3 in ^{73}Kr. The reference values were obtained with level spins equal to those shown in Fig. 1. (b) As (a) but with the spins of bands 1 and 2 reduced by $1\hbar$ (note that this changes the signatures of the bands). Open and solid squares correspond to the two signatures of the negative-parity bands, band 1 $(-,-\frac{1}{2})$ and band 2 $(-,+\frac{1}{2})$, respectively. The solid circles correspond to the positive-parity, positive-signature $(+,+\frac{1}{2})$ band 3.

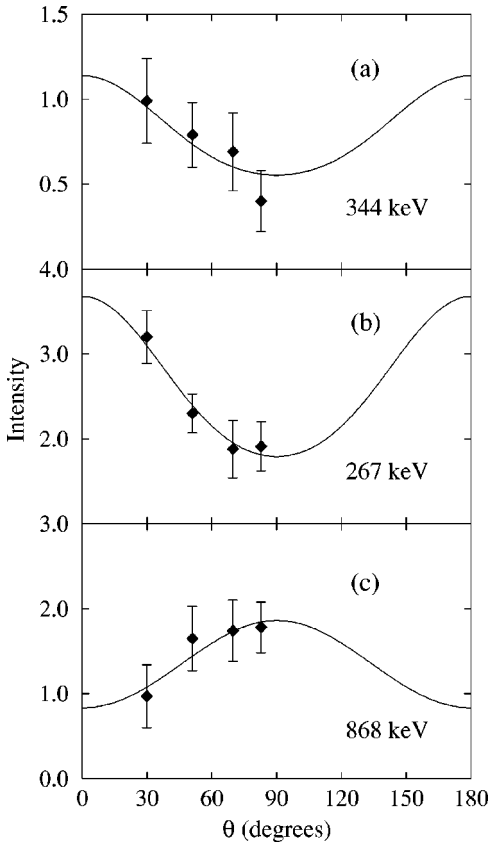

FIG. 5. Angular distribution plots for (a) the 344 keV $\frac{11}{2}^- \rightarrow \frac{9}{2}^-$ transition between bands 1 and 2, (b) the 267 keV $\frac{9}{2}^- \rightarrow \frac{7}{2}^-$ transition between bands 2 and 1, and (c) the 868 keV $\frac{19}{2}^+ \rightarrow \frac{17}{2}^+$ transition between bands 4 and 3. Intensities are given in arbitrary units. See Table II for the mixing ratios obtained from the data.

TABLE II. Measured $\delta(E2/M1)$ mixing ratios obtained from γ-ray angular distributions and calculated $|\delta|(E2/M1)$ mixing ratios determined from branching ratios. The calculated values assume $K=\frac{3}{2}$ for the negative-parity and $K=\frac{5}{2}$ for the positive-parity states. Note that the mixing ratio for the 249 keV transition deduced from angular distributions is likely attenuated due to vacuum deorientation at the bottom of the cascade.

E_γ (keV)	$J_i^\pi \rightarrow J_f^\pi$	$\delta(E2/M1)$ (Angular distributions)	$\lvert\delta\rvert(E2/M2)$ (Branching ratios)
249	$\frac{7}{2}^- \rightarrow \frac{5}{2}^-$	+0.30(9)	0.76(8)
267	$\frac{9}{2}^- \rightarrow \frac{7}{2}^-$	+0.77(12)	0.62(11)
344	$\frac{11}{2}^- \rightarrow \frac{9}{2}^-$	+1.05(29)	1.06(26)
368	$\frac{13}{2}^- \rightarrow \frac{11}{2}^-$	+0.64(23)	0.45(15)
714	$\frac{15}{2}^+ \rightarrow \frac{13}{2}^+$	−0.42(21)	0.65(20)
868	$\frac{19}{2}^+ \rightarrow \frac{17}{2}^+$	−0.29(25)	0.42(12)

achieved. For $K=\frac{3}{2}$ the extracted ratio is a factor of 4 lower than experiment, and for $K=\frac{7}{2}$ it is a factor of 3 larger.

The relative position of $g_{9/2}$ band members near the bandhead is strongly perturbed by Coriolis mixing. This has been studied in detail by Kreiner *et al.* [42]. In a calculation for the positive-parity band in ^{75}Br it was found that the $I^\pi=\frac{5}{2}^+$ and $I^\pi=\frac{9}{2}^+$ members were very closely spaced for axially symmetric prolate deformation. In particular, for $0.3<\beta_2<0.35$ the $\frac{5}{2}^+$ state is less than 100 keV below the $\frac{9}{2}^+$ state. This also appears to be the situation in ^{73}Kr. Thus, all of the observed properties of the band—its level ordering, the branching ratios, the angular distributions, and, as we will discuss below, the alignments—are consistent with a near-prolate band with $\beta\sim0.35$ and having the $[422]\frac{5}{2}$ Nilsson configuration as its dominant amplitude. The inference that the ^{73}Kr bands are near prolate, despite strong shape coexistence in even-even neighbors, is consistent with the observations in the $N=37$ isotone ^{72}Br [43,44].

IV. DISCUSSION

The bands observed in the present work have been compared to predictions of the pairing-and-deformation self-consistent total Routhian surface (TRS) model [45–47] and to the cranked Nilsson-Strutinsky (CNS) approach [48]. Both models are based on the macroscopic-microscopic method of Strutinsky [49]. The Routhian $E'(\omega,\beta_2,\gamma,\beta_4)$ at fixed frequency ω or the energy $E(I,\varepsilon_2,\gamma,\varepsilon_4)$ at fixed angular momentum I is minimized with respect to the quadrupole (β_2/ε_2 and γ) and hexadecapole (β_4/ε_4) deformation parameters. The TRS model uses a Woods-Saxon single-particle potential, while the CNS approach is based on the Nilsson potential with the parameter set from Ref. [50]. In addition, calculations in the frame of the cranked relativistic mean field (CRMF) theory [51] have been carried out employing the NL3 force [52].

Pairing is neglected in the CNS and CRMF calculations; therefore, the results are expected to be realistic only at high rotational frequency. However, the TRS model takes the proton-proton and neutron-neutron pair correlations into account by employing a combination of the conventional monopole and doubly stretched quadrupole pairing interactions [45]. Approximate particle-number projection is facilitated by means of the Lipkin-Nogami method [45,53]. Further details of the models may be found in Refs. [45–48,51].

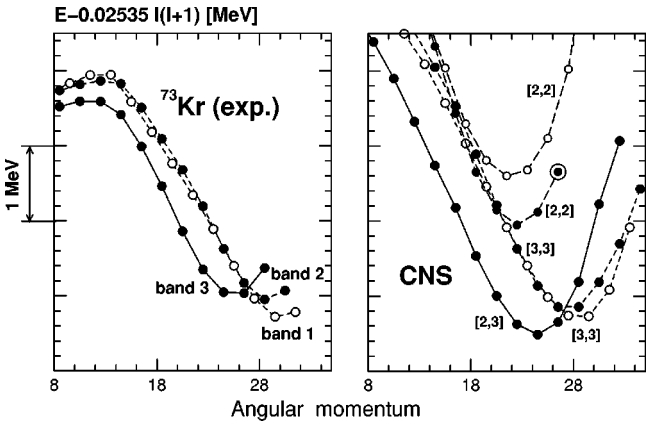

FIG. 6. Excitation energies E of the experimental bands 1–3 in ^{73}Kr [panel (a)] and configurations calculated in the CNS model [panel (b)] as a function of angular momentum given relative to a rigid rotor reference [$E_{RLD}=0.02535I(I+1)$ MeV]. Calculated terminating states are encircled. Solid lines are used for parity $\pi=+$, while short-dashed and long-dashed lines are used for $\pi=-$. Solid circles are used for signature $\alpha=+1/2$ and open circles for $\alpha=-1/2$. Note that at low spin oblate or near-oblate ($\gamma\sim-60°$) configurations are calculated to be lower in energy but they are not shown because the observed experimental properties clearly suggest that the low-spin states are prolate; see Sec. III.

A. Comparison of data with the CNS and CRMF models

At rotational frequencies $\omega\geqslant1.0$ MeV/$\hbar$, bands 1–3 exhibit features that appear typical for the unpaired regime of

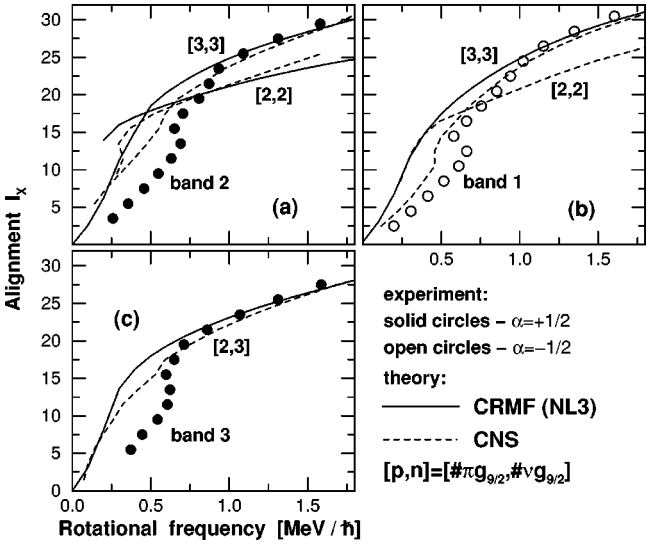

FIG. 7. Plot showing the total angular momentum along the rotation axis I_x, as a function of rotational frequency for experimental bands and calculated configurations from the CNS and CRMF calculations. The notation of the lines and symbols is given in the figure.

rotation influenced by the limited angular momentum content available within each configuration. These are a decreasing kinematic moment of inertia $J^{(1)}$ with increasing rotational frequency and a smooth drop of the dynamic moment of inertia $J^{(2)}$ with increasing ω to values much lower than $J^{(1)}$. Such features have previously been seen in smooth terminating bands (see Refs. [48,54]) and in the super- and highly deformed bands of the $A\sim 60$ mass region [55]. In both cases, calculations without pairing have been rather successful in explaining the observed properties. In order to identify the configurations discussed, we will quote the number of particles in the relevant orbitals. Since all high-j $f_{7/2}$ orbitals are occupied in the configurations of interest, we count only mixed low-j $N=3$ orbitals and use the pf label. A subscript $[\cdots]_U$ is used in order to distinguish these single-particle configurations from the quasiparticle configurations, which will be used below. We also use the shorthand notation $[p,n]$, which indicates the number $p(n)$ of occupied $g_{9/2}$ proton (neutron) orbitals.

Figures 6(a) and 6(b) show the experimental and calculated level energies relative to a rigid rotor reference (E_{RLD}) as a function of spin. Although the CNS calculations indicate the existence of low-lying, aligned (terminating) states in the spin range of interest, only the collective configurations, $[\pi(pf)^6(g_{9/2})^2\otimes\nu(pf)^6(g_{9/2})^3]_U=[2,3]$ and $[\pi(pf)^5(g_{9/2})^3\otimes\nu(pf)^6(g_{9/2})^3]_U=[3,3]$, which are lowest in energy at high spin ($I\approx 20\hbar-30\hbar$), are shown in Fig. 6(b). In addition, the two signatures of the configuration $[\pi(pf)^6(g_{9/2})^2\otimes\nu(pf)^7(g_{9/2})^2]_U=[2,2]$ are displayed. Since the results of the CRMF calculations are very similar to the ones presented in Fig. 6(b), they are not shown. From the figure, one can see that for spin $I\geqslant 14\hbar$, there is clearly good agreement between experiment and theory for all three bands. Indeed the slopes, the positions of the minima in the $(E-E_{RLD})$ curves, and the relative excitation energies are well reproduced in the calculations. Note that the energy splitting between bands 1 and 2 and its increase at $I\geqslant 28\hbar$ are nicely reproduced by the $[3,3](\alpha=\pm 1/2)$ configurations. This correspondence suggests that at high spin the configuration [2,3] can be assigned to band 3 and the $[3,3](\alpha=\pm 1/2)$ configurations to bands 1 and 2.

The experimental and calculated aligned angular momenta, denoted by I_x, are compared in Fig. 7. The spin values of band 3 are well reproduced in the CNS and CRMF calculations for $\omega\geqslant 0.7$ MeV/$\hbar$, while for bands 1 and 2 good agreement between theory and calculations is observed at $\omega\geqslant 1.0$ MeV/$\hbar$. The level of agreement obtained for these bands at high spin is comparable to the agreement seen in similar calculations for nuclei away from the $N=Z$ line (see Ref. [48] and references quoted therein), in the $A\sim 60$ mass region [55] and in ^{74}Kr [56] and ^{72,73}Br [27,44]. The fact that the results of the calculations without pairing, using two completely different approaches, are very close to experiment might suggest that pairing correlations (including np $T=0$ pairing correlations) are rather weak or that they do not lead to considerable modifications of the rotational properties at very high spins. This will be discussed further in Sec. IV B 4 below.

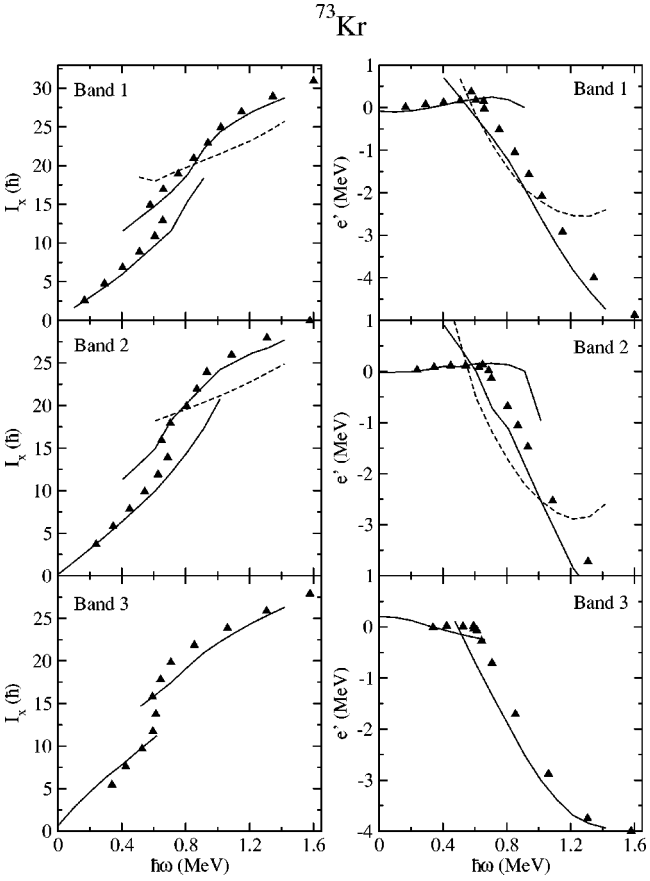

FIG. 8. The plots on the left show the experimental and theoretical I_x values as a function of rotational frequency for bands 1, 2, and 3 in ^{73}Kr while those on the right show the Routhians e' for the same bands calculated using Harris parameters of $\mathcal{J}^{(0)}=18\hbar^2$ MeV^{-1} and $\mathcal{J}^{(1)}=0\hbar^4$ MeV^{-3}. Solid symbols show the experimental data points while the solid and dashed lines show the results of the TRS calculations for the configurations discussed in the text. For bands 1 and 2 the projection of the angular momentum on the deformation axis, K, was taken as $\frac{3}{2}$ while for band 3 a value of $\frac{5}{2}$ has been used. The calculations have been normalized to the low spin portion of the data for band 1.

B. Comparison of data with the TRS model

In the presence of pairing, we use the common cranked shell model notation. We label the configurations by quoting the quasiparticles excited from the ground band, and in order to avoid confusion with the unpaired calculations, the subscript $[\cdots]_P$ is added.

The TRS calculations predict a highly deformed, near-prolate shape for all of the observed bands at low spins. The quadrupole deformation is $\beta_2\sim 0.38$ at low spins and the γ values of the two lowest bands with $(\pi,\alpha)=(-,-\frac{1}{2})$ and $(-,\frac{1}{2})$ from the configuration $[\nu(pf)]_P$ are $\sim 9°$ and $-12°$, while the values for the lowest $(\pi,\alpha)=(+,\frac{1}{2})$ and $(+,-\frac{1}{2})$ bands from the $[\nu g_{9/2}]_P$ configuration are $\gamma\sim 2°$ and $4°$, respectively. This agrees well with both the conclusions of the present work and that of Freund *et al.* [30], who stated that no evidence for large oblate deformation could be

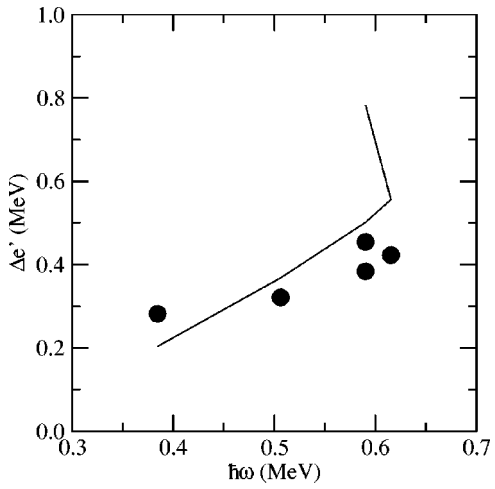

FIG. 9. Comparison of experimental (solid dots) and theoretical (TRS model, solid line) signature splitting as a function of rotational frequency ($\hbar\omega$) for the $\nu g_{9/2}$ band (band 3) in ^{73}Kr.

found below a spin of $\frac{17}{2}$ in their work.

Figure 8 presents the experimental and theoretical values of the total angular momentum along the rotation axis I_x and the Routhians e' as a function of rotational frequency ($\hbar\omega$) for bands 1–3 in ^{73}Kr. It can be seen from these plots that two of the three bands (bands 1 and 3) experience an alignment at a rotational frequency of $\sim$0.62 MeV/$\hbar$ and that for the remaining band (band 2) the alignment occurs at $\sim$0.66 MeV/$\hbar$. In addition, the negative-parity bands appear to undergo a second very gradual alignment at $\sim$0.9 MeV/$\hbar$. The solid lines in Fig. 8 show the calculated values of I_x and the Routhians e' for the lowest-energy configurations for each of the bands as detailed below and in the figure caption. Clearly, the calculated spins below the band crossings agree with the experimental data.

1. Positive-parity states

For the favored signature of the $[\nu g_{9/2}]_P$ band (band 3) one expects that only a pair of $g_{9/2}$ protons will align, since the equivalent $g_{9/2}$ neutron alignment is Pauli blocked. The $g_{9/2}$ proton alignment is predicted to occur $\sim$0.12 MeV below the experimentally observed crossing frequency. It is also noticeable from the I_x plot that the calculations do not yield the correct alignment gain at the band crossing. However, the calculated and experimental spins do converge at higher frequencies. The TRS predicts that the deformation of this band will be reduced from $\beta_2 \sim 0.37$ at low frequencies ($\omega \leqslant 0.5$ MeV/$\hbar$) to a value of $\beta_2 \sim 0.30$ after the $\pi g_{9/2}$ alignment. However, the nucleus is expected to remain approximately prolate at all frequencies, with values of the triaxial deformation parameter γ lying between 2° and 3°.

Unfortunately, the data for band 4 do not extend through the first alignment. Assuming that band 4 is the signature partner, it is possible to compare the experimental and theoretical signature splitting for the band up to the band crossing region. (We note that band 4 could be based upon a different configuration to that assumed in this work.) As seen in Fig. 9, the TRS reproduces the experimental signature splitting quite well up to the start of the $g_{9/2}$ proton alignment.

2. Negative-parity states

The calculations predict a well-deformed ($\beta_2 \sim 0.39$) near-prolate shape for both of the negative-parity bands at low spins. The triaxiality parameter γ is predicted to be $\sim 9°$ at low rotational frequency (<0.5 MeV) for the $(\pi,\alpha)=(-,-\frac{1}{2})$ band, while for the $(\pi,\alpha)=(-,\frac{1}{2})$ band it is $\sim -12°$. This difference in γ values can be traced to different admixtures of the $p_{3/2}$ and $f_{5/2}$ orbitals in the configurations of the two bands, the former favoring positive γ values while the latter favors negative values.

The calculated values of I_x and e' for bands 1 and 2 are shown in Fig. 8 along with the experimental values. One should note that the calculations have been normalized to the data for the $(\pi,\alpha)=(-,-\frac{1}{2})$ configuration at low spin (i.e., before the $g_{9/2}$ band crossings). These bands were previously assigned to the configuration $[\nu(pf)]_P$ based on the two signatures of the $[312]\frac{3}{2}$ Nilsson orbital. The TRS model predicts that there is a simultaneous alignment of a pair of $g_{9/2}$ protons and a pair of $g_{9/2}$ neutrons for both signatures at $\omega \sim 0.53$ MeV/$\hbar$. After these band crossings, the configuration becomes $[\pi(g_{9/2})^2 \otimes \nu(pf)(g_{9/2})^2]_P$ (dashed line in Fig. 8). As in ^{74}Kr, the alignment of $g_{9/2}$ particles results in a shape change towards smaller quadrupole deformation. It is clear from Fig.8, however, that although this configuration is much lower in energy than the continuation of the $[\nu(pf)]_P$ configuration, it clearly fails to reproduce the experimental data, since the calculated spins are too low when compared to experiment.

The CNS and CRMF calculations suggest that bands 1 and 2 have a [3,3] configuration at high spin. A paired configuration with this composition is the three-quasiparticle configuration $[\pi(pf)g_{9/2} \otimes \nu g_{9/2}]_P$. The properties of this configuration are also shown in Fig. 8, as a solid line extending to high rotational frequencies. This configuration, which is found to be yrast at very high spin, nicely accounts for the experimental data. Hence we tentatively assign this configuration to the high-spin part of bands 1 and 2. The slight increase in aligned angular momenta, which can be seen in both bands around $\hbar\omega \sim 0.9$ MeV, can be explained in terms of a decrease in quadrupole deformation, which results in an increase of the alignment of the $g_{9/2}$ protons and neutrons. The calculated quadrupole deformation drops from $\beta_2 \sim 0.35$ to 0.29 near this frequency and, with increasing frequency, there is a further small reduction of the deformation to $\beta_2 = 0.28$ and $\gamma = 7°$ at $\hbar\omega = 1.4$ MeV.

Although the two alternative configurations $[\pi(pf)g_{9/2} \otimes \nu g_{9/2}]_P$ and $[\pi(g_{9/2})^2 \otimes \nu(pf)(g_{9/2})^2]_P$ have the same parity, one would expect them to form two very distinct bands, with essentially no interaction between them, since they differ by *both* the change of a quasiproton from negative to positive parity and the creation of a pair of quasineutrons with positive and negative parities. Exchanging quasiprotons with quasineutrons, the same type of excitation exists between the one-quasineutron configuration $[\nu(pf)]_P$ before the band crossing and the $[\pi(pf)g_{9/2} \otimes \nu g_{9/2}]_P$ configura-

tion. Hence, if the $[\pi(pf)g_{9/2}\otimes\nu g_{9/2}]_P$ assignment is correct, the present data reveal an unusual bandcrossing. The conventional picture describes the backbending mechanism in terms of $T=1$ pairing, where a pair of high-j like particles is broken and aligns, which would correspond to a change from the $[\nu(pf)]_P$ configuration to the $[\pi(g_{9/2})^2\otimes\nu(pf)\times(g_{9/2})^2]_P$ configuration. Here, however, we suggest a configuration change from $[\nu(pf)]_P$ to $[\pi(pf)g_{9/2}\otimes\nu g_{9/2}]_P$, which may also involve the $[\pi(g_{9/2})^2\otimes\nu(pf)(g_{9/2})^2]_P$ configuration as an intermediate step. The relatively smooth change in moment of inertia observed in the band crossing region could indicate the presence of strong mixing between the three- and five-quasiparticle configurations discussed above. Such a mixing may indicate the presence of static $T=0$ pairing correlations since the configurations are related by the exchange of a neutron-proton pair from identical pf-shell orbitals into identical $g_{9/2}$ orbitals. A measurement of the lifetimes in the crossing region would be of great interest since one could then determine whether the transitions are enhanced or retarded.

Our association between the paired and unpaired configurations is based on the comparison of the TRS and CRMF/CNS calculations. The alignment properties of corresponding configurations are similar at high spins (compare Figs. 7 and 8). The fact that the [2,2] configurations are not seen in the experimental data may be explained by the mixing with other configurations, as discussed in the preceding paragraph. However, there are alternative explanations: for example, they may not be fed because they lie far away from the yrast line at the spin where the feeding takes place, or they may terminate before this spin (see Fig. 6).

3. Band crossing frequencies

In previous work, the TRS model was found to account well for all of the observed bands in the $T_z=1$ nucleus ^{74}Kr [4]. However it could not account for the properties of the yrast band structure in ^{72}Kr [2,18] and, in particular, for the delay in alignment in the yrast sequence. The authors suggested that np pairing may be the reason for the discrepancy in the $N=Z$ nucleus. In the case of ^{73}Kr (see Fig. 8), the calculated $g_{9/2}$ proton and neutron crossing frequencies are generally lower ($\sim$0.1 MeV) than the experimental data. However, the magnitude of the disagreement appears to be less than for the yrast band of ^{72}Kr [2,17,18]. This may be related to the increase of the neutron number N by 1.

In order to see if there is such a trend, we compared TRS calculations with data in ^{75}Kr (taken from Ref. [10]), which is three neutrons away from the $N=Z$ line. Figure 10 shows I_x and e' for the favored signatures of the positive- and negative-parity bands. The TRS calculations appear to reproduce the experimentally observed crossing frequencies somewhat better in this case. Thus, taking into account the excellent agreement between calculations and the experimental data in ^{74}Kr, ^{78}Sr, and ^{82}Zr [4] it would seem that, from this limited comparison, the TRS model is more successful at predicting the experimental crossing frequencies in nuclei which are not too close to the $N=Z$ line. This may suggest that the model lacks some important physics when trying to describe the $N=Z$ nuclei. Neutron-proton pairing seems to be the favorite candidate at the present time.

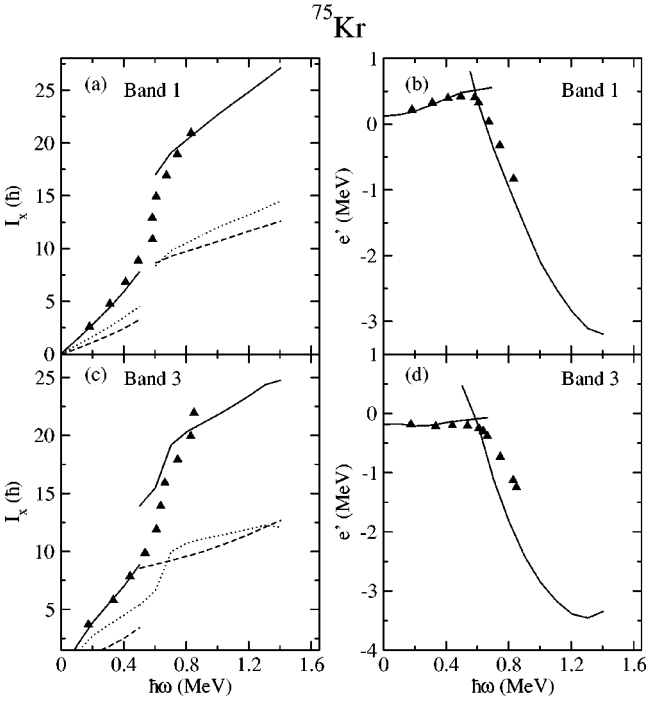

FIG. 10. The plots on the left show the experimental and theoretical I_x values as a function of rotational frequency for bands 1 and 3 in ^{75}Kr while those on the right show the Routhians e' for the same bands calculated using Harris parameters of $\mathcal{J}^{(0)}=18\hbar^2$ MeV^{-1} and $\mathcal{J}^{(1)}=0\hbar^4$ MeV^{-3}. Solid symbols show the experimental data points while the solid lines show the results of the TRS calculations. The dashed and dotted lines represent the calculated neutron and proton contributions to I_x, respectively. For the $g_{9/2}$ band (band 3) a K value (projection of the angular momentum on the deformation axis) of $\frac{5}{2}$ has been used. The calculations have been normalized to the low-spin portion of the data from band 1.

4. Evidence for np pairing?

While the band crossing frequency argument presented above does not provide strong evidence for np pairing in nuclei such as ^{73}Kr at high spin, we believe that the new data, along with other data in this region, give at least an indication that such pairing may be necessary in $T_z=0,\pm\frac{1}{2}$ nuclei in order to yield an accurate description. However, the question of whether pair correlations of $T=0$ or of $T=1$ character cause the shifts remains unanswered.

A number of calculations [57–59] suggest that there may be $T=0$ pairing at high spin. Since there is no Coriolis antipairing effect for $T=0$ np pairs, this type of pairing might survive up to very high spin if the coupling strength is sufficiently strong. One may therefore expect that deviations between calculations without pairing and high-spin data in $N\sim Z$ nuclei may indicate the presence of isoscalar ($T=0$) np pairing. At first sight one would therefore suggest that the lack of any such deviations in the present work might indicate that all pairing (including $T=0$ pairing) is rather weak

at high spins. However, as shown in Ref. [57], even if there are substantial $T=0$ static pairing correlations present, they may not show up in the experimental data. Hence, this would suggest that from the present data set we cannot make any firm conclusions on the presence or absence of $T=0$ correlations at high spin from such a comparison.

The unusual transition from the one- to the three-quasiparticle configuration, instead of the expected five-quasiparticle configuration, seen in the negative-parity bands may be considered as possible evidence for substantial $T=0$ pair scattering, provided our configuration assignment is correct. However, one should also note that a similar kind of band crossing has been seen before in nuclei far away from the $N=Z$ line (e.g., ^{156}Dy for example, Refs. [60,61]). In this case the ground-state band, which has the standard vacuum configuration at low spin, terminates around spin $60\hbar$ with an odd number of $h_{11/2}$ protons and $i_{13/2}$ neutrons in the configuration. This would suggest that at intermediate spins there is a band crossing of a similar type to that observed in ^{73}Kr.

Finally, a further word of caution is necessary. The details of the calculated bands, such as the crossing frequencies and the alignments, depend on how accurately the single-particle spectra are reproduced. Since the single-particle potentials in the case of the TRS and CNS calculations and the effective force in the case of CRMF calculations have not been optimized for the present mass region, it may not be surprising that some differences between the calculations and the experiment occur. Moreover, it is well known that crossing frequencies and other rotational characteristics are sensitive to the triaxiality and quadrupole deformation parameters, which are only calculated but not yet confirmed by experiment. Hence, at the present time it is difficult to determine how much of the disagreement in the crossing frequencies between theory and experiment can be attributed to the lack of np pairing in the models and how much should be assigned to the uncertainty of the nuclear shape.

V. CONCLUSIONS

In summary, we have revised and greatly extended the previously known decay scheme for the $N=Z+1$ nucleus ^{73}Kr. The three known bands have been extended up to spins of $\frac{63}{2}^-$ (band 1), $\frac{61}{2}^-$ (band 2), and $\frac{57}{2}^+$ (band 3). In addition, a new positive-parity band (band 4), which is believed to be the signature partner to band 3, has been identified up to a tentative spin of $\frac{31}{2}^+$. Measured mixing ratios indicate prolate deformation at low spin for both the negative- and positive-parity bands.

The bands have been discussed in terms of the pairing-and-deformation self-consistent TRS model, the cranked Nilsson-Strutinsky model, and the relativistic mean-field theory. At high spin, all three models give very similar results and can reproduce quite well the experimental data. The good description of the negative-parity bands by the TRS model appears to result from a band crossing at $\hbar\omega \sim 0.6$ MeV which is very different from the familiar backbending mechanism. Calculations suggest that two bands are involved and that the configurations of the crossing bands ($[\pi(g^{9/2})^2 \otimes \nu[[(fp)(g^{9/2})^2]_P$ and $[\pi(fp)(g_{9/2}) \otimes \nu[[(g_{9/2})]_P$) are related by the exchange of a neutron-proton pair from the pf orbit into the $g_{9/2}$ orbit. The relatively smooth behavior of the moments of inertia might suggest that these distictly different configurations are mixed. A possible source of such mixing could be the presence of $T=0$ pair correlations.

The TRS model has problems in reproducing the band crossing frequencies in several $N=Z$ nuclei (e.g., ^{72}Kr, ^{76}Sr, and ^{80}Zr), whereas it appears to work somewhat better for $T_z=1$ nuclei (e.g., ^{74}Kr, ^{78}Sr, and ^{82}Zr). The present study of a $T_z=\frac{1}{2}$ nucleus adds further evidence to this trend. The crossing frequencies in the yrast positive- and negative-parity bands in the $N=Z+3$ nucleus ^{75}Kr appear to be better reproduced than those in the $N=Z+1$ nucleus ^{73}Kr. This feature may be an indication that the TRS model, which uses the standard pairing acting only between like nucleons, lacks some important physics for the complete description of $T_z=0,\pm\frac{1}{2}$ nuclei. Neutron-proton pair correlations could be the missing ingredient.

Further tests of the models are necessary to determine if the high-spin data contain evidence for the np pair correlations. It will be important, for example, to determine the deformation of the various rotational structures both before and after the $g_{9/2}$ proton and neutron band crossings in order to study the effects of shape changes on the crossing frequencies. Lifetime measurements in this region will therefore be required since they will help determine how the nuclear deformation changes with spin within a given configuration.

ACKNOWLEDGMENTS

The authors would like to thank the staff at the ATLAS accelerator for providing the beam and John Greene for manufacturing the targets. This work was supported by the U. K. EPSRC, U. S. NSF, and Department of Energy under Contract Nos. DE-AC03-76SF00098, DE-FG02-95ER40934, and W-31-109-ENG38. R. M. C. and R. W. also wish to acknowledge support from NATO. S.M.F. acknowledges support from the Research Corporation.

[1] B.J. Varley *et al.*, Phys. Lett. B **194**, 463 (1987).
[2] G. de Angelis *et al.*, Phys. Lett. B **415**, 217 (1997).
[3] W. Korten *et al.*, Acta Phys. Pol. B **32**, 729 (2001).
[4] D. Rudolph *et al.*, Phys. Rev. C **56**, 98 (1997).
[5] C. Chandler *et al.*, Phys. Rev. C **56**, R2924 (1997).
[6] F. Becker *et al.*, Eur. Phys. J. A **4**, 103 (1999).
[7] S.M. Fischer, D.P. Balamuth, P.A. Hausladen, C.J. Lister, M.P. Carpenter, D. Seweryniak, and J. Schwartz, Phys. Rev. Lett. **84**, 4064 (2000).
[8] A. Algora *et al.*, Phys. Rev. C **61**, 031303(R) (2000).
[9] S. Skoda *et al.*, Z. Phys. A **336**, 391 (1990).
[10] S. Skoda *et al.*, Nucl. Phys. **A633**, 565 (1998).

[11] A.O. Macchiavelli *et al.*, Phys. Rev. C **61**, 041303(R) (2000).
[12] A.O. Macchiavelli *et al.*, Phys. Lett. B **480**, 1 (2000).
[13] S. Frauendorf and J. Sheihk, Nucl. Phys. **A645**, 509 (1999).
[14] W. Satuła and R. Wyss, Phys. Lett. B **393**, 1 (1997).
[15] W. Satuła and R. Wyss, Phys. Rev. Lett. **86**, 4488 (2001).
[16] W. Satuła and R. Wyss, Phys. Rev. Lett. **87**, 052504 (2001).
[17] S.M. Fischer *et al.*, Phys. Rev. Lett. **87**, 132501 (2001).
[18] N.S. Kelsall *et al.*, Phys. Rev. C **64**, 024309 (2001).
[19] N. Marginean *et al.*, Phys. Rev. C **63**, 031303 (2001).
[20] J. Sheikh and R. Wyss, Phys. Rev. C **62**, 051302(R) (2000).
[21] R. Wyss, in *Nuclei Far From Stability and Astrophysics*, edited by D. N. Poenaru *et al.* (Kluwer Academic, Dordrecht, 2001), pp. 139–149.
[22] R. Wyss and W. Satuła, in *Proceedings of the Warsaw Meeting on High Spins*, edited by J. Dobaczewski (Kluwer Academic, Dordrecht, 2001).
[23] C.J. Gross *et al.*, Phys. Rev. C **56**, R591 (1997).
[24] S.D. Paul *et al.*, Phys. Rev. C **58**, R3037 (1998).
[25] A.V. Afanasjev, D.B. Fossan, G.J. Lane, and I. Ragnarsson, Phys. Rep. **322**, 1 (1999).
[26] F. Cristancho *et al.*, Phys. Lett. B **357**, 281 (1995).
[27] C. Plettner *et al.*, Phys. Rev. C **62**, 014313 (2000).
[28] M. Satteson *et al.*, J. Phys. G **16**, L27 (1990).
[29] D.M. Moltz *et al.*, Nucl. Phys. **A526**, 111 (1993).
[30] S. Freund *et al.*, Phys. Lett. B **302**, 167 (1993).
[31] Ch. Miehe, Ph. Dessagne, Ch. Pujol, G. Walter, B. Jonson, M. Lindroos, and the ISOLDE Collaboration, Eur. Phys. J. A **5**, 143 (1999).
[32] C. Chandler *et al.*, Phys. Rev. C **61**, 044309 (2000).
[33] P. Hausladen, Ph.D. University of Pennsylvania, 1998.
[34] I.Y. Lee, Nucl. Phys. **A520**, 641c (1990).
[35] D.G. Sarantites *et al.*, Nucl. Instrum. Methods Phys. Res. A **381**, 418 (1996).
[36] D. Seweryniak *et al.*, Nucl. Instrum. Methods Phys. Res. A **340**, 353 (1994).
[37] D.C. Radford, Nucl. Instrum. Methods Phys. Res. A **361**, 297 (1995).
[38] K.S. Krane *et al.*, Nucl. Data Tables **A11**, 351 (1973).
[39] K.S. Krane and R.M. Steffen, Phys. Rev. C **2**, 724 (1970).
[40] K. Nakai, Phys. Lett. **34B**, 269 (1971).
[41] C.J. Lister *et al.*, Phys. Rev. Lett. **49**, 308 (1982).
[42] A.J. Kreiner *et al.*, Phys. Rev. C **24**, 148 (1981).
[43] S. Ulbig *et al.*, Z. Phys. A **329**, 51 (1988).
[44] C. Plettner *et al.*, Phys. Rev. Lett. **85**, 2454 (2000).
[45] W. Satuła, R. Wyss, and P. Magierski, Nucl. Phys. **A578**, 45 (1994).
[46] W. Satuła and R. Wyss, Phys. Rev. C **50**, 2888 (1994).
[47] W. Satuła and R. Wyss, Phys. Scr. **T56**, 159 (1995).
[48] A.V. Afanasjev, D.B. Fossan, G.J. Lane, and I. Ragnarsson, Phys. Rep. **322**, 1 (1999).
[49] V.M. Strutinsky, Yad. Fiz. **3**, 614 (1966).
[50] D. Galeriu, D. Bucuresku, and M. Ivasku, J. Phys. G **12**, 329 (1986).
[51] A.V. Afanasjev, J. König, and P. Ring, Nucl. Phys. **A608**, 107 (1996).
[52] G.A. Lalazissis, J. König, and P. Ring, Phys. Rev. C **55**, 540 (1997).
[53] H.C. Pradhan, Y. Nogami, and J. Law, Nucl. Phys. **A201**, 357 (1973).
[54] A.V. Afanasjev and I. Ragnarsson, Nucl. Phys. **A591**, 387 (1995).
[55] A.V. Afanasjev, I. Ragnarsson, and P. Ring, Phys. Rev. C **59**, 3166 (1999).
[56] A. V. Afanasjev and S. Frauendorf (unpublished).
[57] A.L. Goodman, Phys. Rev. C **63**, 044325 (2001).
[58] W. Satula and R. Wyss, Nucl. Phys. **A676**, 120 (2000).
[59] J. Terasaki, R. Wyss, and P.H. Heenan, Phys. Lett. B **437**, 1 (1998).
[60] J. Simpson *et al.*, Nucl. Phys. **A486**, 35 (1988).
[61] F.G. Kondev *et al.*, Phys. Lett. B **437**, 35 (1998).